# Sensing current and forces with SPM

Atomic force microscopy (AFM) and scanning tunneling microscopy (STM) are well established techniques to image surfaces and to probe material properties at the atomic and molecular scale. In this review, we show hybrid combinations of AFM and STM that bring together the best of two worlds: the simultaneous detection of atomic scale forces and conduction properties. We illustrate with several examples how the detection of forces in STM and the detection of currents in AFM can give valuable additional information of the nanoscale material properties.

**Jeong Y. Park[1,2], Sabine Maier[1], Bas Hendriksen[1], and Miquel Salmeron[1,3,*]**

[1] *Materials Sciences Division, Lawrence Berkeley National Laboratory, University of California, Berkeley CA 94720*

[2] *Current address: WCU Program, Graduate School of EEWS, Korea Advanced Institute of Science and Technology (KAIST), Daejeon, Republic of Korea*

[3] *Materials Science and Engineering Department, University of California, Berkeley CA 94720*

**E-mail: mbsalmeron@lbl.gov*

**Did you ever touch a doorknob after walking on carpet on a dry day? If you did, you probably sensed two properties in a single touch: the physical contact, i.e. the doorknob is solid, and the unpleasant feeling of the electrical discharge, informing you that the doorknob is a conductor. In this paper, we review selected examples of such combined mechanical and electrical sensing experiments at the atomic and molecular scale using two branches of scanning probe microscopy (SPM): atomic force and scanning tunneling microscopy.**

The idea of measuring forces and current (as illustrated in Fig. 1a) with a sharp metallic tip attached to a cantilever can be traced back to the invention of the atomic force microscope by G. Binnig *et al.*[1]. When a sharp probe tip, mounted on a cantilever (spring), is scanned over the surface, forces acting between the tip and the sample surface induce a displacement of the tip, by bending the cantilever. In the initial design of an AFM, the bending of the cantilever was measured by the most sensitive position detection method available, i.e. by measuring the tunneling current between a metallic tip and the backside of the cantilever. This tunneling current depends exponentially on the tip-sample separation; here the sample is the backside of the cantilever. Scanning a tip over a surface while maintaining a constant current and tip-sample separation forms the basis of STM imaging (as shown in Fig. 1a).

Currently, one of most widely used force detection schemes in AFM is the beam deflection method invented by Meyer and Amer[2]. In this setup, a laser beam is reflected from a micro-machined cantilever. The reflected laser beam is detected with a position-sensitive quadrant detector that allows measuring both the bending (normal force) and the torsion (lateral force) of the cantilever, as illustrated in Fig. 1b. If a conductive tip and cantilever are utilized, the electrical current between the tip and the sample can be measured simultaneously and independently. The concept of a combined scanning tunneling



ISSN:1369 7021 © Elsevier Ltd 2010
Open access under CC BY-NC-ND license.

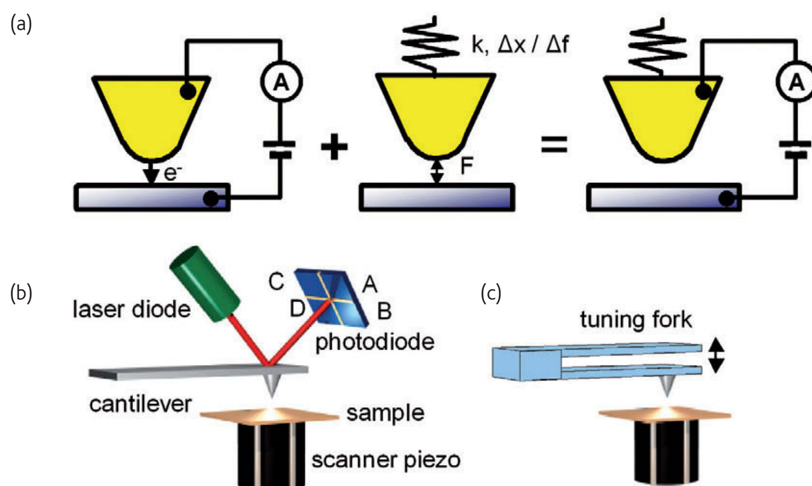


*Fig. 1 Hybrid STM and AFM. (a) The concept of combining STM and AFM to simultaneously measure currents and forces at the atomic scale. (b) Force detection by cantilever deflection provides normal and lateral forces, and (c) tuning fork dynamic force detection provides normal force gradients.*

microscope/atomic force microscope[3-5] is shown schematically in Fig. 1a. This scheme allows for the study of not only surface structure but also charge transport and mechanical properties of surfaces and interfaces at the atomic or molecular scale. Two types of force/current sensors are mainly used: micro-machined cantilevers and tuning forks. While the force detection by cantilever deflection provides normal and lateral forces (Fig. 1b), tuning fork force detection provides normal force gradients (Fig. 1c). Measurements of lateral forces with tuning forks require a different mounting, as will be described later.

A combined AFM/STM can be operated in static and dynamic modes, depending on which feedback signal is used for tip-sample distance control. In the next three sections, we will outline the different operation modes of combined AFM/STM and some of their applications in surface science.

## Probing tip-surface forces in scanning tunneling microscopy

When one images surfaces with a heterogeneous electronic structure, variations of tip-sample forces have a significant influence on the image contrast[3,5]. Understanding the interaction between the STM tip and the substrate surface is therefore very important for accurate image analysis and characterization of these electrically distinct regions, such as semiconductor devices and organic molecules on metallic surfaces. Tip-sample force interactions can be probed in STM mode by collecting the tunneling current with a conducting AFM cantilever. While the tunneling current is used for the tip-sample distance feedback control, the tip-sample force interaction is measured simultaneously by monitoring the cantilever bending. To ensure stable tunneling, cantilevers or probes with high spring constant (> 50 N/m) were used to suppress jump-to-contact instabilities.

Many efforts have been made to characterize tip-sample forces during scanning tunneling microscopy. On metals and highly doped semiconductors the forces during non-contact tunneling are attractive because the tip remains relatively far away from the surface[6]. Due to poor electrical conductivity in lightly doped semiconductors or in insulating layers, however, the tip might come very close to, or might even come in direct contact with the surface, giving rise to a strong repulsive force[7,8].

Initial investigations of the tip-surface interaction by measuring forces during STM imaging focused on graphite, because its atomic lattice can be easily resolved in air. Sugawara *et al.*[4] observed repulsive forces indicative of contact and surface conductance during STM/AFM imaging. Freshly etched tungsten and platinum levers were used for sensing tip-surface forces in constant current STM mode. Similarly, the forces acting between a Pt-Rh tip and graphite surface were studied by Mate *et al.*[9].

Grigg et al. measured such repulsive force between a W probe and Pt grating surfaces in STM mode using a rocking beam force balance sensor[10] and concluded that surface contaminants repelled the probe from the underlying Pt. It was observed that the repulsive forces between probe and tip lead to elastic or inelastic deformations in the area under the tip and therefore have important effects on imaging. Salmeron et al. reported anomalous topographical corrugation (elastic deformation) and permanent damage (inelastic deformation) during STM imaging of a graphite surface indicating the effect of compressive and shear forces[11]. Pi *et al.* observed irreversible deformation on the alkylthiol self-assembled monolayers due to the repulsive tip-surface interaction[12].

By simultaneous topographic and force measurements with a combined STM/AFM, the strength of the electric field produced by dipoles at atomic steps was measured on Pt(111), Au(111) and Al-Ni-Co quasicrystal surfaces as shown in the scheme of Fig. 2a[13]. Figs. 2c and 2d show the STM topography and force image of Pt(111) obtained simultaneously for a tip bias of –0.2 V and Fig. 2b the

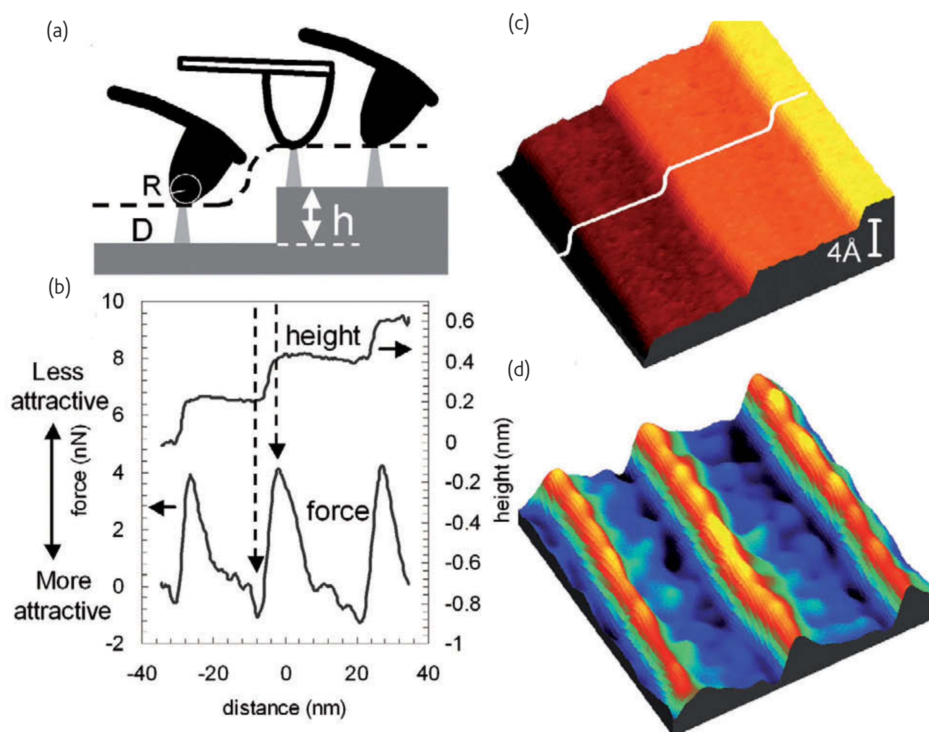


*Fig. 2 (a) STM-AFM configuration using a conductive cantilever bending in response to forces. (b) Height and force profile across the steps. The force on the tip is more attractive at the bottom of the steps and less attractive at the top. (c) The 70 nm x 70 nm STM image and (d) force imaging of a Pt(111) surface (Vt = -0.2 V, I=0.16 nA). Yellow and blue colors represent low and high attractive forces, respectively. (Reprinted figure with permission from [13]. © 2005 by the American Physical Society.)*

corresponding height and force profiles. The force was always found to be attractive and increased by ~1.5 nN as the tip approached the bottom of the step and decreased by ~4 nN on the upper terrace. When the attractive force increased, the STM current feedback loop retracted the base of the cantilever to keep the tunnel current, and hence the tip-sample distance, constant. The cantilever deflection provided a direct measurement of the forces on the tip when crossing the step. The reduction of the attractive force in the upper side of the steps was due to the reduction in the van der Waals and polarization part of the force (image charges). This was a consequence of the fact that at the position of the step the lower terrace is farther away from the tip. The contribution of the step dipole was separated from changes in the force due to van der Waals and polarization forces by varying the tip-sample bias.

It is well known that on electrically non-uniform surfaces, such as semiconductors, variations of electrostatic forces during non-contact atomic force microscopy (AFM) imaging lead to a strong bias dependence in topographical images[14]. In STM imaging of electrically heterogeneous surfaces similar effects exist. Force variations on a silicon pn junction were investigated during STM imaging[8]. It was found that in an attempt to keep the tunneling current constant while crossing the pn junction on the n-area at reverse bias the tip pressed against the surface to draw the set-point current, while it was in non-contact tunneling regime at the forward bias on the p side of the junction.

The mechanical interaction between a scanning tunneling microscopy probe and a self-assembled monolayer of organic molecules was investigated by sensing the force during STM imaging[15] as shown in Fig. 3. A Au(111) surface was partially covered by hexadecane (C16) alkylthiol molecules forming islands. Fig. 3a shows the schematic of the STM tip scanning over the gold surface and the molecular islands, with simultaneous force mapping. Depending on the current setpoint, the tip was in full contact with the molecules, which produces a backward bending of the lever. Figs. 3b and 3c show STM and force images acquired simultaneously using a sample bias of 2 V. The dark circular areas in Fig. 3b represent 1 nm deep depressions corresponding to the alkylthiol islands, with typical lateral dimensions of 20–50 nm. The STM image is a plot of the variation of the length of the piezoactuator supporting the sample during scanning. In normal STM operation, where the tip is rigid, this produces a 'topographic' image, which is dominated by the reduced conductivity of the islands and therefore does not represent true topography. In the present case, however, the lever is bending due to variations in the normal force. A compensated STM image with tip height profile can be obtained by compensating STM topography with lever bending to reconstruct a topography image. In this manner it was found that the interaction between the tip and the C16 alkylthiol molecules goes from non-contact to contact at 1 pA and 2 V sample bias, which is comparable to the calculated threshold tunneling current by Bumm *et al.*[7].

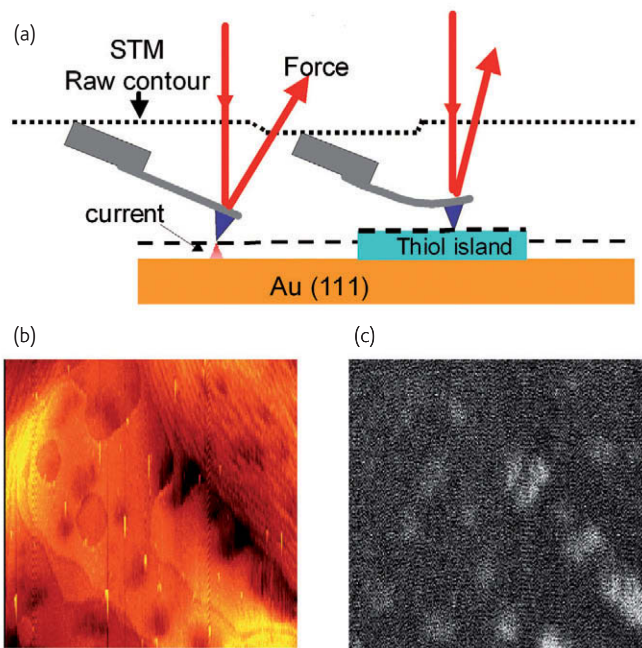


*Fig. 3 (a) Schematic of an AFM tip scanning over a surface of Au covered with islands of alkylthiol molecules. (b) 300 x 300 nm² STM image acquired with a conductive AFM tip in STM mode at 2 V and 10 pA and (c) Tip-sample force map acquired simultaneously. The bright and dark areas in the force map represent repulsive and attractive forces respectively (Reprinted figure with permission from[15]. © 2008 by the American Physical Society.)*

## Probing tip-surface currents in atomic force microscopy (static mode)

Conductive AFM (C-AFM)[16], another hybrid STM/AFM mode, is basically no more than using electrically conductive AFM tips connected to a current pre-amplifier during conventional contact-mode AFM, using the cantilever (normal) deflection as the feedback signal to regulate the tip-substrate distance. When a bias voltage is applied between the conducting tip and a conducting substrate, one obtains the corresponding current signal. The tip-sample current is an additional independent signal that allows for conductance probing and mapping of samples with conducting and insulating areas or domains. This makes C-AFM particularly useful to study electrically inhomogeneous substrates. There are numerous studies using C-AFM and, rather than providing a complete review we briefly discuss a few examples and describe some experiments from our own laboratory in more detail.

C-AFM can obtain lattice resolution. For example, Enachescu *et al*. have used tungsten carbide coated AFM tips to image the topography, friction and current on HOPG and graphene layers on Pt (111) (See Fig. 4a)[17]. The current level was in the range of nA-mA and revealed the lattice-resolved image of the carbon atoms. It was also shown that the current level on the lower side of the step was reduced from 39 μA to 28 μA (see Figure 4b) while the AFM topography is completely flat at the same area and does not reveal the presence of a step in the graphite layer. The authors suggested that the high resolution was due to the fact that only a small fraction of the tip-sample contact was electrically conducting, much smaller than the physical contact area.

C-AFM[18,19] and break-junction experiments[20-23] are two of the tools for studying the conduction properties of organic monolayers. In most tip-monolayer-substrate junctions of C-AFM, the self-assembled monolayer (SAM) simply acts as a tunneling barrier, albeit with a reduced barrier compared to a vacuum gap of the same thickness. This is because the (tails of) HOMO-LUMO molecular levels assist electron transfer by non-resonant tunneling through the molecular monolayer[24]. External forces that cause molecular deformation and conformation changes can influence charge transport properties of conducting molecules. The capability of probing electrical and mechanical properties with nanoscale resolution makes SPM a very useful and promising tool in studying charge transport properties through molecules which, with adequate theoretical support could provide invaluable information into molecular bonding deformation mechanisms giving rise to changes in electronic levels and current. The field of molecular electronics, for example, benefits enormously from the use of C-AFM to measure local conductivity in organic films and its dependence on local molecular structure and geometry, applied forces and the effect of gating bias voltages that change the electronic level positions.

It was found that the electron tunneling process through alkylthiol self-assembled monolayers on a gold substrate depends strongly on

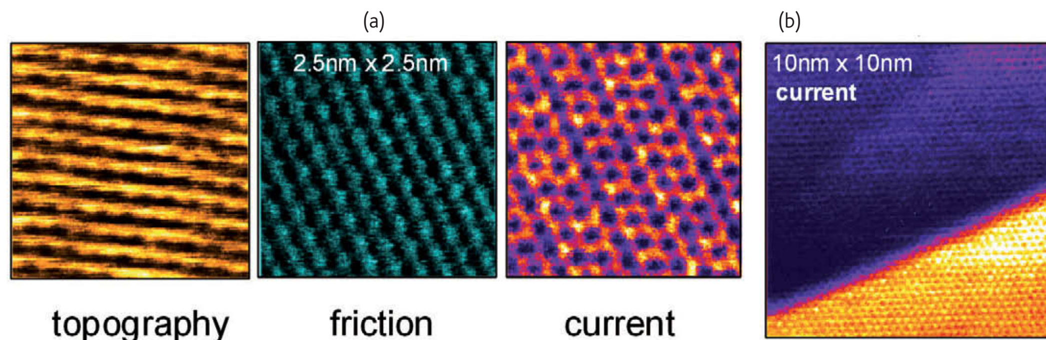


*Fig. 4 (a) Topography, friction and current mapping acquired at an applied load of 300 nN with no feedback and a bias of 0.53 V. (b) C-AFM current image of a Pt step covered by a contiguous layer of graphite measured at a bias of 1.0 V. The topography image (not shown) is completely flat, and does not reveal the presence of a step in the graphite layer at this scale. (Reprinted figure with permission from[17]. ©1999 by the American Physical Society.)*

the tilt angle of the alkane chains[25-27]. The tilt angle was varied by applying an increasing load by the tip on the SAM while simultaneously measuring the tunnel current (see Fig. 5). It was suggested that when the tile angle increases, electrons might tunnel not only along the backbone of the molecules but also across neighboring molecules on their way from the tip to the substrate[26]. A similar 'two-pathway' tunneling model[28] was found to be consistent with the conduction through alkyl silane SAM[29]. On the other hand, as pointed out for alkylthiols on a gold substrate[25], distortions of the molecular bonds, particularly those between the S end and Au, could also produce changes in the tunneling current when tilting forces the S atom to change even slightly its position. Based on the load dependence of the conduction through SAM of aromatic molecules, Fang *et al.* suggested that intermolecular π-orbital transport is involved in the tip-SAM-substrate conduction[30]. Wold *et al.* have determined that the length dependence of the conduction through conjugated oligophenylene SAMs is much weaker than through saturated alkane SAMs[31]. The same was found by Sakaguchi *et al.*[32]. Leatherman *et al.* studied the conduction of conjugated carotene wires embedded in an alkanethiol SAM[33]. More recently Choi *et al.* used C-AFM to determine the resistance of long conjugated molecular wires and found a transition of direct (nonresonant) tunneling to hopping transport through the molecular wire depending on the length of the wire[34]. By space charge limited current measurements with C-AFM and modeling, Reid *et al.* could extract reliable charge carrier mobilities of various conjugated polymers[35]. Cui *et al.* used gold nano particles to create reliable contacts to alkanedithiols, which do not depend on the applied force. By scaling and binning the obtained IV curves, they could distinguish transport through single molecule contacts[36]. Photo-switching of the electrical conductance of azobenzene derivatives was observed with C-AFM by Mativetsky[37]. IV spectroscopy using C-AFM is not limited to materials relevant to molecular/organic electronics. The IV characteristics of biological molecules, such as photosynthetic complexes and other proteins, have been studied as well[38-40].

Most C-AFM experiments described so far focused on the determination of the IV characteristics. However, current imaging or mapping is also a very useful method to determine spatial variations in the conductance. For example, Yang *et al.* found that the structure and connectivity of pentacene layers strongly affects their lateral conduction[41]. Sutar *et al.* used C-AFM current mapping and IV spectroscopy to study the conduction properties of polyaniline micro-crystalline heterostructures[42]. Blends of organic polymers (polyaniline and PMMA) have been studied by Planès *et al.*[43]. Li *et al.* imaged multi-walled carbon nanotubes that were vertically embedded in $SiO_2$ by current mapping[44].

Conductive AFM tips were used as a local probe electrode to contact molecular islands of sexithiophene crystals and water polymerized polypyrol[45-47]. The conduction of a DNA network in contact with gold electrodes has been imaged as a function of humidity[48]. Resistance mapping of carbon nanotubes in contact with an electrode has been performed by several groups[49,50]. Paulson *et al.* pushed carbon nanotubes with the AFM tip, causing them to rotate in and out of registry with the lattice of the underlying graphite substrate. Subsequent conduction measurements of the carbon nanotubes with the C-AFM tip revealed that when the tube was commensurate with the graphite the resistance was minimized[51]. Nakamura *et al.* used a conducting AFM tip as the source electrode to contact copper phthalocyanine nano-crystals in a field effect transistor (FET) geometry[52]. Yaish *et al.* used an Au coated AFM tip as a nanoprobe to measure the resistance of a nanotube in a FET geometry[53]. Seshadri and Frisbie used an Au coated AFM tip to perform potentiometry of an operating sexithiophene based FET[54].

The use of C-AFM is obviously not limited to organic materials. The electrical properties of a variety of inorganic materials have been studied with C-AFM. Examples include ultrathin layers of $SiO_2$[55-57], $TiO_2$[58], polycrytalline ZnO[59], ZnO nano rods[60], Cr films on SiC[61], Au nanostructures[62], GaMnAs structures[63], CdTe nano-tetrapods[64], etc. In addition to the use of C-AFM for local electrical probing, the tip can be used for nanopatterning. Electrical fields and currents applied by the C-AFM tip have been used to locally oxidize structures[65,66], to write

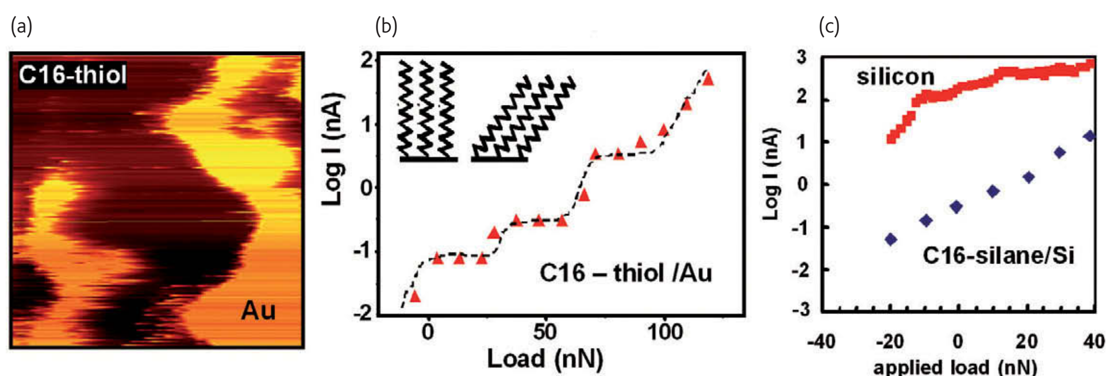


*Fig. 5 (a) 600 nm x 600 nm current image of a gold sample partially covered with C16 alkylthiols at a bias of 1.5 V. (b) Semilog plot of the current measured on C16 alkylthiols (at 1 V bias) and (c) on C16-silanes in $SiO_2$/Si as function of the applied load (at -0.8V). The plateaus revealed in (b) are associated with discrete tilt angle of the molecules. (Reprinted figure with permission from[25,29]. © 2009 by the American Physical Society and © 2008 by the American Chemical Society.)*

patterns in SAM[67] or to inject charges locally, to anchor nanoparticles, i.e., the nanoscale equivalent of the Xerox process[68].

In the examples given above, the conducting AFM was only used as a local electrical probe. Recent work by Chang et al. is an example that truly exploits the combined force and current detection[69]. These researchers detected the attractive forces between pairs of guanine-cytosine and adenine-thymine molecules, one molecule of the pair adsorbed on the tip and the other one in a SAM on the substrate. The molecules of the pair interacted through hydrogen bonds and the tunneling current was measured through those hydrogen bonds by C-AFM. The authors used the C-AFM force and current data to construct an electromechanical model describing the role of stiffness of the (STM)-(molecule)-(hydrogen bond)-(molecule)-(substrate) junction in their separate STM-based transport measurements for molecular recognition.

Contact-mode AFM is a powerful tool to study the nanoscale friction properties of materials (friction force microscopy, FFM)[70]. When conducting tips are used in AFM friction experiments, the effect of electronic components of friction can be studied. An example of such effects is illustrated by the recent report of the electronic friction properties of planar silicon pn junctions[71]. In this study a conducting TiN AFM tip was scanned over a planar pn junction covered with a thin oxide layer. There was no noticeable difference in the friction between the p-type and the n-type area of the silicon substrate at zero sample bias. However when a positive sample voltage was applied, the friction on the p-type area was higher compared to the n-type area (see Fig. 6). At positive sample voltage the p-type area was in forward bias, i.e. holes accumulated in the area under the tip, and the n-type area was in reverse bias, i.e. electrons were depleted. Although the current was higher on the forward-biased p-type area it was found that the friction was actually independent of the current value between the tip and the sample. In a separate study Qi et al. found a similar electronic effect on n-type GaAs covered with an ultrathin oxide[72]. An asymmetry was found in the friction force while scanning the GaAs at forward bias and reverse bias. Consistent with the Si pn junctions, the friction was found to be higher at forward bias. A charge trapping model was suggested to explain the observed magnitude of the friction force, its bias dependence, and the scanning velocity dependence. According to this model, charges get trapped in the oxide covering the GaAs only in forward bias leaving a slowly decaying trail of charges behind the tip that exert an electrostatic pull on the tip that is manifested as an increases in the friction force. The electromechanical properties of ferroelectric materials are widely studied with piezoresponsive force microscopy (PFM)[73]. In PFM, a conductive AFM tip is used to apply an AC voltage to the ferroelectric material. The resulting piezoresponse of the ferroelectric, i.e. the mechanical response to the applied voltage, is detected in the lateral force signal, i.e. the torsional response of the AFM cantilever. In this way, domains of different piezoelectric polarization orientation can be resolved. By applying a sufficiently high DC voltage, the orientation of the domains can be switched reversibly and patterns can be written. Recently, Seidel *et al.* have shown by C-AFM that the domain walls separating piezoelectric domains in $BiFeO_3$ films are electrically conductive, whereas the domains themselves are insulating[74].

The reliability of C-AFM measurements strongly depends on the quality of the C-AFM tips and various conducting coatings including Pt, Au, TiN and $W_2C$ have been evaluated[75-78]. It is generally found that AFM tips coated with metal films fail after some time of use because the metal coating wears off. Fein *et al.* used tapping mode AFM with a conductive tip to measure the current during the short time of contact[79]. Operating C-AFM in tapping mode reduces the shear forces on the tip, which allowed the tips to last longer. On the other hand, inspection of Pt-coated silicon tips used in our lab for current imaging revealed the formation of a thin film of organic molecules that caused reduction of the conductivity of the AFM tip. Reliable C-AFM imaging on hard sample surface requires the coating of hard materials on the tip because the soft coating materials can be easily peeled off upon contact with the hard material. If the hardness of tip coating material is much higher than that of sample surface, it results in plastic deformation or scratching on the sample surface. Therefore, the choice of materials for the tip coating would be a key factor of reliable operation of C-AFM.

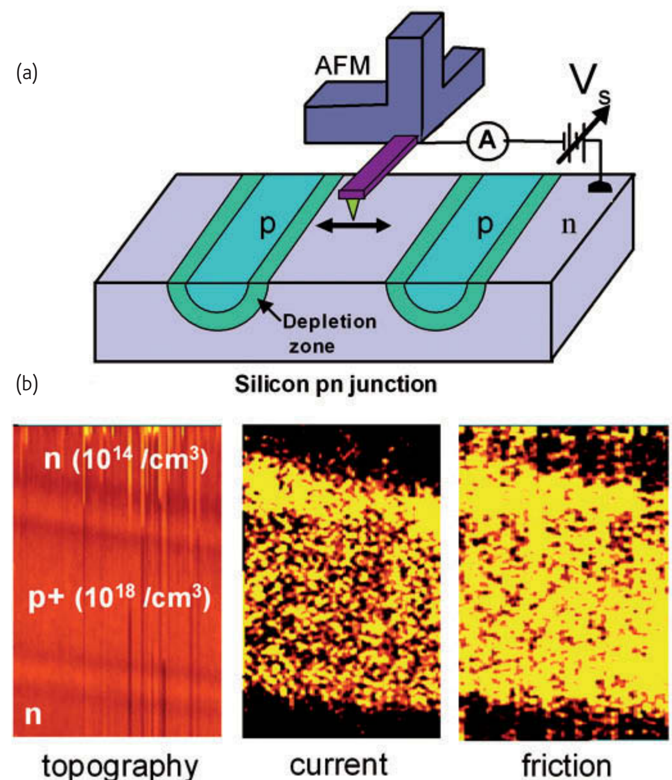


*Fig. 6 (a) Schematic of friction and current measurements on a silicon pn junction device with a C-AFM and (b) 3.5 x 5.0 μm² topography, current, and friction images of a region containing a stripe of p-type Si at +4 V bias. The p region is forward biased (strong accumulation), and the n region reverse biased. The applied load was 8 nN and the scanning speed was 5 μm/second. (Figures adapted from[77]) (Reprinted figure with permission from[71]. © 2006 by AAAS.)*

## Probing tip-surface currents in atomic force microscopy (dynamic mode)

The combination of force and current sensing has been successfully extended to dynamic non-contact AFM/STM. By using metal-coated or highly-doped silicon cantilevers, the current has been monitored during frequency modulated (FM) and amplitude modulated (AM) noncontact AFM on conductive samples. In FM-AFM, this operation mode has been used to better understand the imaging contrast on surfaces at the atomic level. For example Enevoldsen et al. modeled the tip structure during the imaging of a $TiO_2$(110) surface in combination with atomistic STM simulations based on multiple scattering theory[80]. Inversely, in dynamic STM a time averaged tunnel current between the conducting sample and the oscillating tip can be used to control the probe height above the sample surface. This method combines the high lateral resolution achieved by STM with complementary data on the force gradient. Atomic resolution has been achieved on several conductive samples, such as Si(111)-(7x7)[81,82] and Cu[83] as well as molecular resolution on organic molecules[84,85].

Further, using the tunneling current as a control parameter for the distance to the sample while simultaneously oscillating the tip parallel to the surface makes it possible to determine lateral forces[86,87] However, achieving atomic resolution is difficult due to the large oscillation amplitudes (over tens of nm) required using microfabricated cantilevers. Nonetheless, the attraction and repulsion at a monatomic step could be quantified, as well as the force between sulfur impurities and the tip on a Cu(001) surface[86]. The use of quartz tuning forks as force sensors enables FM-AFM operation with amplitudes of several Angstroms. In this manner, true atomic resolution on a Si(111)-(7x7) surface has been established by showing that both conservative and dissipative force components exhibit clear variations on the atomic scale as shown in Fig. 7a and 7b[87].

At a temperature of 4K, thermal drift rates are small and allow simultaneous high-resolution measurements of tunneling current and frequency shift at constant tip-sample distance. In these operating conditions, quartz tuning forks are common sensors and can provide enhanced sensitivity to short-range forces. In this way, Hembacher *et al*. studied the atomic structure of a graphite (0001) surface in great detail. Combined STM/AFM experiments using the frequency modulation force microscopy method, with the cantilever oscillating at a fixed amplitude revealed the 'hidden' atoms in the unit cell[88,89]. Fig. 7c and 7d show constant-height dynamic mode STM image and a constant-height dynamic AFM image, respectively, which reveal two types of atoms forming the basis of the hexagonal surface unit cell, $\alpha$ (white) and $\beta$ (red). While only the $\beta$ atoms appear in the STM image (Fig. 7c), the dynamic mode AFM image (Fig. 7d) shows both $\alpha$ and $\beta$ atoms.

Recently, the forces required to pull individual adsorbates along a surface have been quantified using the same technique[90]. Ternes *et al*. have shown that moving single cobalt (Co) atoms on Pt(111) require a lateral force of 210 pN, independent of the vertical force, while about 17 pN were sufficient to manipulate Co atoms on Cu(111). These results clearly show that the required force to move an atom strongly depends on the supporting substrate.

## Conclusion and outlook

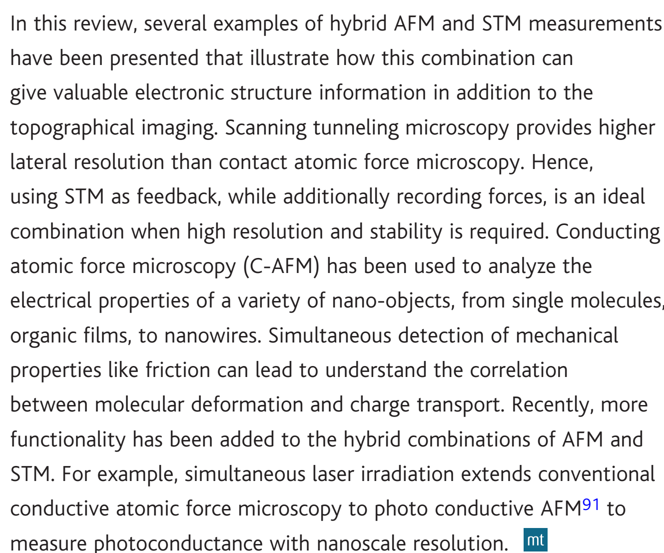

In this review, several examples of hybrid AFM and STM measurements have been presented that illustrate how this combination can give valuable electronic structure information in addition to the topographical imaging. Scanning tunneling microscopy provides higher lateral resolution than contact atomic force microscopy. Hence, using STM as feedback, while additionally recording forces, is an ideal combination when high resolution and stability is required. Conducting atomic force microscopy (C-AFM) has been used to analyze the electrical properties of a variety of nano-objects, from single molecules, organic films, to nanowires. Simultaneous detection of mechanical properties like friction can lead to understand the correlation between molecular deformation and charge transport. Recently, more functionality has been added to the hybrid combinations of AFM and STM. For example, simultaneous laser irradiation extends conventional conductive atomic force microscopy to photo conductive AFM[91] to measure photoconductance with nanoscale resolution. mt

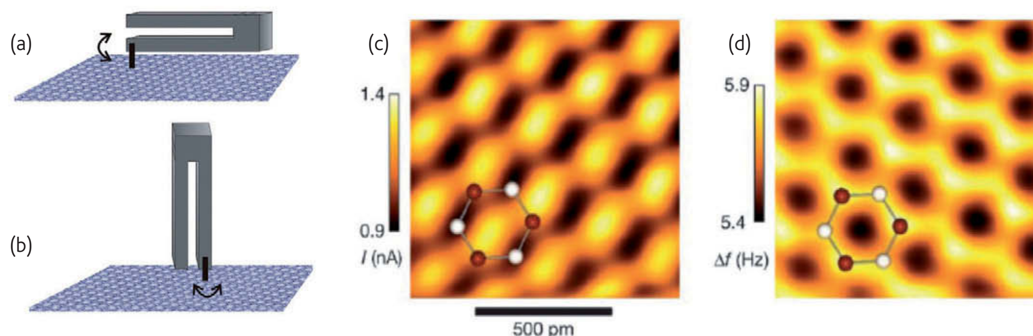


*Fig. 7 (a) Schematics of normal and (b) lateral force detection using a tuning fork as a force sensor. (c) Constant-height dynamic mode STM image of graphite (bias voltage 100 mV, amplitude 300 pm, scanning speed 0.2 nm/s), and (d) constant-height dynamic AFM mode simultaneously recorded with (c). (Reprinted figure with permission from[88]. © 2003 by PNAS.)*

## Acknowledgements

*This work was supported by the Director, Office of Science, Office of Basic Energy Sciences, Materials Sciences and Engineering Division, of the U.S. Department of Energy under Contract No. DE-AC02-05CH11231. J.Y.P. acknowledges the partial support by WCU (World Class University) program through the National Research Foundation of Korea funded by the Ministry of Education, Science and Technology (31-2008-000-10055-0).*



**REFERENCES**

1. Binnig, G., *et al., Phys Rev Lett* (1986) **56**, 930.
2. Meyer, G., and Amer, N. M., *Appl Phys Lett* (1988) **53**, 1045.
3. Anselmetti, D., *et al., J. Vac. Sci. Technol. B* (1994) **12**, 1677.
4. Sugawara, Y., *et al., J. Vac. Sci. Technol. B* (1991) **9**, 1092.
5. Tang, S. L., *et al., Appl Phys Lett* (1988) **52**, 188.
6. Durig, U., *et al., Phys Rev Lett*1986, **57**, 2403.
7. Bumm, L. A., *et al., J Phys Chem B* (1999) **103**, 8122.
8. Park, J. Y., *et al., Appl Phys Lett* (2005) **86**, 172105.
9. Mate, C. M., *et al., Surf Sci* (1989) **208**, 473.
10. Grigg, D. A., *et al., J. Vac. Sci. Technol. A* (1992) **10**, 680.
11. Salmeron, M., *et al., J. Vac. Sci. Technol. B* (1991) **9**, 1347.
12. Pi, U. H., *et al., Surf Sci* (2005) **583**, 88.
13. Park, J. Y., *et al., Phys Rev Lett* (2005) **95**, 136802.
14. Sadewasser, S., and Lux-Steiner, M. C., *Phys Rev Lett*(2003) **91**, 266101.
15. Park, J. Y., *et al., Journal of Chemical Physics* (2008) **128**, 234701.
16. *Various names for this mode exist depending on authors and AFM manufacturers: conduction AFM (C-AFM), current-sensing AFM (CS-AFM), conducting-probe AFM (CP-AFM), tunneling AFM (TUNA), scanning spreading resistance microscopy (SSRM).*
17. Enachescu, M., *et al., Phys Rev B* (1999) **60**, 16913.
18. Salmeron, M., *et al., Langmuir* (1993) **9**, 3600.
19. Klein, D. L., and McEuen, P. L., *Appl Phys Lett* (1995) **66**, 2478.
20. Reed, M. A., *et al., Science* (1997) **278**, 252.
21. Kergueris, C., et al., *Phys Rev B* (1999) **59**, 12505.
22. Xu, B. Q., and Tao, N. J. J., *Science* (2003) **301**, 1221.
23. Reddy, P., *et al., Science* (2007) **315**, 1568.
24. Wang, W. Y., *et al., Rep Prog Phys* (2005) **68**, 523.
25. Qi, Y. B., *et al., Langmuir* (2008) **24**, 2219.
26. Song, H., *et al., J Am Chem Soc* (2007) **129**, 3806.
27. Wold, D. J., and Frisbie, C. D., *J Am Chem Soc* (2001) **123**, 5549.
28. Slowinski, K., *et al., J Am Chem Soc* (1997) **119**, 11910.
29. Park, J. Y., *et al., Journal of Chemical Physics* (2009) **130**, 114705.
30. Fang, L., *et al., Langmuir* (2007) **23**, 11522.
31. Wold, D. J., *et al., J Phys Chem B* (2002) **106**, 2813.
32. Sakaguchi, H., *et al., Appl Phys Lett* (2001) **79**, 3708.
33. Leatherman, G., *et al., J Phys Chem B* (1999) **103**, 4006.
34. Choi, S. H., *et al., Science* (2008) **320**, 1482.
35. Reid, O. G., *et al., Nano Letters* (2008) **8**, 1602.
36. Cui, X. D., *et al., Science* (2001) **294**, 571.
37. Mativetsky, J. M., *et al., J Am Chem Soc* (2008) **130**, 9192.
38. Stamouli, A., *et al., Febs Letters* (2004) **560**, 109.
39. Xu, D. G., *et al., Nano Letters* (2005) **5**, 571.
40. Zhao, J. W., et al., *J Am Chem Soc* (2004) **126**, 5601.
41. Yang, H. C., *et al., J Am Chem Soc* (2005) **127**, 11542.
42. Sutar, D. S., *et al., Organic Electronics* (2008) **9**, 602.
43. Planes, J., *et al., Appl Phys Lett* (2001) **79**, 2993.
44. Li, J., *et al., Appl Phys Lett* (2002) **81**, 910.
45. Kelley, T. W., *et al., Advanced Materials* (1999) **11**, 261.
46. Loiacono, M. J., *et al., J Phys Chem B* (1998) **102**, 1679.
47. Yamamoto S. I., and Ogawa, K., *Surf Sci* (2006) **600**, 4294.
48. Terawaki, A., *et al., Appl Phys Lett* (2005) **86**, 113901.
49. Dai, H. J., *et al., Science* (1996) **272**, 523.
50. Otsuka, Y., *et al., Appl Phys Lett* (2003) **82**, 1944.
51. Paulson, S., *et al., Science* (2000) **290**, 1742.
52. Nakamura, M., *et al., Thin Solid Films* (2003) **438**, 360.
53. Yaish, Y. *et al., Phys Rev Lett*(2004) **92**, 046401.
54. Seshadri, K., and Frisbie, C. D., *Appl Phys Lett* (2001) **78**, 993.
55. Frammelsberger, W., *et al., Applied Surf Sci* (2006) **252**, 2375.
56. Olbrich, A., *et al., Appl Phys Lett* (1998) **73**, 3114.
57. O'Shea, S. J., *et al., J. Vac. Sci. Technol. B* (1995) **13**, 1945.
58. Boxley, C. J., *et al., J Phys Chem B* (2003) **107**, 9677.
59. Shao, R., *et al., Appl Phys Lett* (2003) **82**, 1869.
60. Schlenker, E., *et al., Phys Status Solidi B* (2007) **244**, 1473.
61. Mazur, P., *et al., Vacuum* (2007) **82**, 364.
62. Bietsch, A., *et al., J. Vac. Sci. Technol. B* (2000) **18**, 1160.
63. Farshchi, R., *et al., Physica B* (2007) **401**, 447.
64. Fang, L., *et al., J Chem Phys* (2007) **127**, 184704.
65. Snow, E. S., and Campbell, P. M., *Science* (1995) **270**, 1639.
66. Wilder, K., *et al., Appl Phys Lett* (1998) **73**, 2527.
67. Kramer, S., *et al., Chem Rev* (2003) **103**, 4367.
68. Seemann, L., *et al., Nano Lett* (2007) **7**, 3007.
69. Chang, S., *et al., Nat Nanotechnol* (2009) **4**, 297.
70. Carpick R. W., and Salmeron, M., *Chem Rev* (1997) **97**, 1163.
71. Park, J. Y., *et al., Science* (2006) **313**, 186.
72. Qi, Y. B., *et al., Phys Rev B* (2008) **77**, 184105.
73. Kalinin, S. V., *et al., IEEE T Ultrason Ferr* (2006) **53**, 2226.
74. Seidel, J., *et al., Nat Mater* (2009) **8**, 229.
75. O'Shea, S. J., *et al., Rev Sci Instrum* (1995) **66**, 2508.
76. Trenkler, T., *et al., J. Vac. Sci. Technol. B* (2000) **18**, 418.
77. Park, J. Y., *et al., Physical Review B* (2007) **76**.
78. Enachescu, M., *et al., Journal of Applied Physics* (2004) **95**, 7694.
79. Fein, A., *et al., Appl Phys Lett* (2001) **79**, 3935.
80. Enevoldsen, G. H., *et al., Physical Review B* (2008) **78**, 045416.
81. Güthner, P., *J. Vac. Sci. Technol. B* (1996) **14**, 2428-2431.
82. Lüthi, R., *et al., Phys. B* (1996) **100**, 165-167.
83. Loppacher, C., *et al., Physical Review B* (2000) **62**, 16944-16949.
84. Berdunov, N., *et al., Appl Phys Lett* (2009) **94**, 043110.
85. Loppacher, C., *et al., Appl. Phys. A* (2001) **72**, S105-S108.
86. Pfeiffer, O., *et al., Physical Review B* (2002) **65**, 161403.
87. Giessibl, F. J., *et al., PNAS* (2002) **99**, 12006.
88. Hembacher, S., *et al., PNAS* (2003) **100**, 12539.
89. Hembacher, S., *et al., Phys Rev Lett*(2005) **94**, 056101.
90. Ternes, M., *et al., Science* (2008) **319**, 1066.
91. Lee, J., *et al., Ultramicroscopy* (2008) **108**, 1090.